Development of a Geant4 based Monte Carlo Algorithm to evaluate the MONACO VMAT treatment accuracy

Jens Fleckenstein*, **Lennart Jahnke, Frank Lohr, Frederik Wenz, Jürgen Hesser**

Department of Radiation Oncology, University Medical Center Mannheim, University of Heidelberg, Theodor-Kutzer-Ufer 1-3, 68167 Mannheim, Germany

Received 14 April 2012; accepted 8 August 2012

Abstract

A method to evaluate the dosimetric accuracy of volumetric modulated arc therapy (VMAT) treatment plans, generated with the MONACO^{TM} (version 3.0) treatment planning system in realistic CT-data with an independent Geant4 based dose calculation algorithm is presented.
Therefore a model of an Elekta Synergy linear accelerator treatment head with an MLCi2 multileaf collimator was implemented in Geant4. The time dependent linear accelerator components were modeled by importing either logfiles of an actual plan delivery or a DICOM-RT plan sequence. Absolute dose calibration, depending on a reference measurement, was applied. The MONACO as well as the Geant4 treatment head model was commissioned with lateral profiles and depth dose curves of square fields in water and with film measurements in inhomogeneous phantoms. A VMAT treatment plan for a patient with a thoracic tumor and a VMAT treatment plan of a patient, who received treatment in the thoracic spine region including metallic implants, were used for evaluation.
MONACO, as well as Geant4, depth dose curves and lateral profiles of square fields had a mean local gamma (2%, 2 mm) tolerance criteria agreement of more than 95% for all fields. Film measurements in inhomogeneous phantoms with a global gamma of (3%, 3 mm) showed a pass rate above 95% in all voxels receiving more than 25% of the maximum dose. A dose-volume-histogram comparison of the VMAT patient treatment plans showed mean deviations between Geant4 and MONACO of -0.2% (first patient) and 2.0% (second patient) for the PTVs and (0.5 ± 1.0)%

Entwicklung eines Geant4 basierten Algorithmus zur Evaluierung der MONACO-VMAT-Behandlungsgenauigkeit

Zusammenfassung

Eine Methode zur Evaluierung der dosimetrischen Genauigkeit von MONACO^{TM} (Version 3.0)-VMAT-Behandlungsplänen in realen CT-Datensätzen mittels eines unabhängigen, auf Geant4 basierten Monte-Carlo-Dosisberechnungsalgorithmus wird vorgestellt.
Hierfür wurde ein Modell eines Elekta-Synergy-Linearbeschleunigers mit MLCi2-Kollimator in Geant4 implementiert. Um die zeitlich veränderlichen Komponenten des Beschleunigerkopfes zu modellieren, wurden entweder logfiles einer Bestrahlung oder DICOM-RT-Pläne importiert. Ein auf einer Referenzmessung beruhender Formalismus zur Kalibration der absoluten Dosis wurde angewandt. Sowohl die MONACO- als auch die Geant4-Simulationen wurden mit lateralen Profilen und Tiefendosiskurven quadratischer Feldgeometrien in Wasser und mit Film-Messungen in inhomogenen Phantomen validiert. Ein Vergleich zwischen MONACO- und Geant4-generierten Dosisverteilungen wurde für einen VMAT-Bestrahlungsplan eines Patienten mit einem thorakalen Tumor sowie einen Bestrahlungsplan eines Patienten, der in der Wirbelsäulen-Region in Gegenwart metallischer Implantate bestrahlt wurde, durchgeführt.
Sowohl MONACO als auch Geant4 zeigten für die Tiefendosiskurven und die lateralen Profile der quadratischen

* Corresponding author. Jens Fleckenstein, Department of Radiation Oncology, University Medical Center Mannheim, University of Heidelberg, Theodor-Kutzer-Ufer 1-3, 68167 Mannheim, Germany.
E-mail: Jens.Fleckenstein@medma.uni-heidelberg.de (J. Fleckenstein).

and (1.4 ± 1.1)% for the organs at risk in relation to the prescription dose.
The presented method can be used to validate VMAT dose distributions generated by a large number of small segments in regions with high electron density gradients. The MONACO dose distributions showed good agreement with Geant4 and film measurements within the simulation and measurement errors.

Keywords: Monte Carlo, VMAT, MONACO, Geant4, Commissioning

Felder bei einem lokalen Gamma (2%, 2 mm) Kriterium für alle Felder eine mittlere Übereinstimmung von mehr als 95%. Filmmessungen in inhomogenen Phantomen erfüllten ein globales Gamma (3%, 3 mm) Toleranzkriterium in mehr als 95% aller Voxel, die mehr als 25% der Maximaldosis erhielten. Die Dosis-Volumen-Histogramme der beiden VMAT-Behandlungen zeigten Unterschiede in der mittleren Dosis im Zielvolumen zwischen Geant4 und MONACO von -0,2% im ersten und 2,0% im zweiten Fall. Die Risikoorgane zeigten dosimetrische Unterschiede von (0,5 ± 1,0)% und (1,4 ± 1,1)% bezogen auf die Verschreibungsdosis.
Die vorgestellte Methode kann verwendet werden, um VMAT-Dosisverteilungen, die durch viele kleine Segmente generiert wurden, in Regionen mit großen Elektronendichtevariationen zu verifizieren. Die mit MONACO simulierten Dosisverteilungen zeigten innerhalb der Fehler eine gute Übereinstimmung mit Geant4 sowie den Filmmessungen.

Schlüsselwörter: Monte Carlo, VMAT, MONACO, Geant4, Kommissionierung

Introduction

The Monte Carlo method is considered to be the most accurate form of dose calculation in radiation therapy. It develops its full potential when dose calculations in regions with high electron density gradients have to be performed. Due to a dramatic increase in the efficiency of the available algorithms [1,2] and computation resources, radiotherapy treatment planning with Monte Carlo dose calculation algorithms has become widely available [3] in clinical routine. The clinical Monte Carlo treatment planning system used in this study is MONACO (Elekta, Crawley, UK). To model the fluence generated by the linear accelerator, MONACO is using a virtual energy fluence (VEF) model [4,5] while the dose distribution within the patient is calculated by the Photon Voxel Monte Carlo algorithm XVMC [6,7]. Grofsmid et al. [8] demonstrated the dosimetric accuracy of MONACO (version 1.0) for IMRT cases with static gantry and fixed dose rate by performing measurements in water and anthromorphic phantoms. In order to reduce treatment times MONACO is capable of generating highly modulated VMAT treatment plans with interdigitating MLC leaves [9]. In this treatment modality dose is delivered with up to 240 control points, continuously sweeping over the treatment volume. When delivering dose with sweeping MLC leaves, the dose output of a treatment field not only depends on the number of delivered monitor units (MU), but also on an exact geometric modeling of the MLC and its position [10], especially for off-axis segments. Furthermore a significant amount of dose in highly modulated VMAT treatments may originate from fields smaller than an equivalent square field size of $(3 \times 3)\,\mathrm{cm}^2$. Since the relative errors in penumbra and output factor measurements are higher for small fields [11] errors in the treatment head model may occur. This requires a MONACO VMAT user to perform a thorough analysis of the system prior to clinical usage which will typically either be based on measurements and/ or on an independent Monte Carlo based application [12,13]. Measurements with ionization chamber arrays in water equivalent phantoms are an appropriate tool for VMAT plan verification [14] but may be inaccurate when many small fields are present due to the limited spatial resolution [15,16]. Point detector measurements depend on a precise positioning and show different behavior for small field sizes [17,18]. Radiographic films require a sophisticated evaluation procedure for accurate absolute dose calibration [19,20]. Furthermore all this techniques require a dose-to-medium into dose-to-water conversion [21] when measurements in anthromorphic phantoms are compared to Monte Carlo generated dose distributions. To support the measurement results a comparison of MONACO with an application based on the scientific Monte Carlo class library Geant4 is presented which was used specifically where measurement devices may produce systematic errors: highly modulated VMAT treatment deliveries in inhomogeneous media with a significant amount of dose originating from small off-axis fields. For this evaluation the software toolkit Geant4 [22,23] provided a suitable platform since it was already successfully used for several radiotherapy applications [24–26]. In the implementation presented in this paper, it neither relies on the variance reduction techniques used in the XVMC algorithm, nor makes use of a

VEF model to generate the particle fluence of the treatment head, but explicitly simulates all particle interactions within the treatment head, starting with an electron source upstream of the target.

For the reasons discussed above an evaluation on actual patient geometries with dose volume histograms (DVH) and profile comparisons between dose distributions generated in MONACO and Geant4 was performed in this study. This manuscript describes the development of an application [27,28], that allows the verification of dose distributions of VMAT treatment plans in realistic patient CT data. The obtained results with Geant4 are then compared to dose distributions planned with MONACO in order to validate its dosimetric accuracy for complex treatment deliveries.

Material and methods

The Geant4 application

Monte Carlo simulations were performed with an application based on the software toolkit Geant4.9.4, a C++ based class library. The standard electromagnetic physics packages were used with the Penelope electromagnetic models for photon processes [29] and the Livermore electromagnetic models for lepton processes [30]. The multiple scattering model, used in the simulations, was a condensed algorithm based on the Urban [31] scatter model (G4UrbanMscModel93). A maximum step length of 1 mm was applied to all steps within the scoring geometry. If a particle traversed a voxel boundary within one step, the deposited dose was split according to the relative path length in the respective voxel. Below a range cut of 1 mm, no secondary particles were produced. A DICOM interface based on the DCMtk 3.5.4 (Offis, Oldenburg, Germany) class library was added. The CT data was imported within the DetectorConstruction-class and a three-dimensional grid with $(2 \times 2 \times 2)\,mm^3$ voxel size was created for all presented dose distributions. The DICOM-RT structure file was imported to determine the patient outline. A bounding box around the patient geometry determined the extents of the voxelized geometry. Voxels outside the patient outline were assigned to contain air.

The current linear accelerator settings from an actual plan delivery, specifically the confirmed values of the 80 leaf positions, the 4 jaw positions, the cumulative MU value and the current gantry angle were scored as a function of treatment time with a frequency of 1 Hz in linac logfiles. This data was then used to create static segments. To avoid significant errors due to under-sampling the sampling rate was chosen to not exceed 2° gantry angle, as proposed by Teke et al. [12]. These files were converted into input batch files and were accessed during runtime via appropriate messenger classes for the DetectorConstruction- and the PrimaryGeneratorAction-classes to control the dynamic parts of the treatment head and the particle generation [32]. Furthermore batch files were also generated by converting the contents of a DICOM-RT plan file. A phasespace file (PHSP), containing history information (new history flag, particle type, energy, position and momentum) of the static accelerator parts, was generated once in a plane between the flattening filter and the ionization chambers at 240.0 mm distance from the source. 4.8×10^{10} incident electron histories on the target were simulated with a runtime of (512×11.3) h and 4.6×10^3 histories per second and core (hps), resulting in 2.9×10^9 histories (efficiency $\varepsilon_{source2PHSP} = 6.1\%$) in the PHSP. This phasespace was used to create a patient specific second PHSP at the borders of either a water volume, or the volume containing the CT data information, which was then used for dose calculation. The Geant4 code was parallelized with the openMPI 3.5.4 message passing library [33]. All simulations were performed on the bwGRiD computer cluster[a].

The linear accelerator head model

A geometrical model of an Elekta Synergy linear accelerator treatment head with an MLCi2 multi leaf collimator was implemented in Geant4 according to its construction data. The target with its surrounding copper block, the primary collimator, the flattening filter, the ionization chambers, the backscatter plate, the mylar mirror, the MLC and the two pairs of jaws were modeled with their corresponding material compositions. Each MLC leaf was modeled with six trapezoid surfaces, resulting in a maximum geometrical error of less than 1 mm.

Since the mean incident electron energy predominantly influenced the shape of the central axis depth dose curve, as well as the shape of the lateral profiles [34,35], an analysis of seven different mean incident electron energies between 5.8 MeV and 6.8 MeV was performed. An initial electron point source with a kinetic energy of $E = (6.7 \pm 0.2)$ MeV was positioned 30 mm upstream of the target [35,34] and had a divergence, such that it created a Gaussian shaped spot with $\Delta d_{fwhm} = 1.9$ mm on the target surface ($\Theta_{FWHM} = 66.6$ mrad). Only electrons with energies inside an energy window of $E_{cut} = \pm 0.6$ MeV were accepted, to model the energy filtering through the bending magnets. In the simulation the spatio-temporal behavior of the MLC leaves and the two jaw pairs were modeled according to the vendor's construction data and MLC dynamic of an ideal linear accelerator.

Dose scoring and absolute dose calibration

The number of histories per control point (CP) from the first phasespace was kept constant for all control points to obtain a comparable standard deviation. From the resulting field-sequence specific phasespace, the histories were recycled 4-8

[a] bwGRID (http://www.bw-grid.de), member of the German D-Grid initiative, funded by the ministry of education and research and the ministry for science, research and arts Baden-Wuerttemberg, Germany.

times to simulate the dose distribution. During the simulation of the dose distribution of one control point, the energy deposit in a voxel was scored with Sempau's method [36] to minimize memory allocation and simulation time. After the histories of one control point were simulated, the mean energy deposit per incident electron $\overline{E}_{i,j}$ in a voxel j with density ρ_j and volume V_j was converted to dose and multiplied with the number of monitor units MU_i of the current control point and an absolute dose calibration factor c_{abs} according to equation (1).

$$D_j = \frac{c_{abs}}{V_j \rho_j} \times \sum_{i=1}^{CP} (\overline{E}_{i,j} \times MU_i) \tag{1}$$

The reference dose was determined in a reference simulation of a $(10 \times 10)\,cm^2$ square field at SSD = 100 cm [37,38]. The ratio c_{abs} of the dose deposit D_{sim}^{ref} in a $(0.4 \times 0.4 \times 0.4)\,cm^3$ volume at the central axis in 10 cm depth and an absolute dose measurement D_{meas}^{ref} of an equivalent setup and 200 MU was determined to be

$$c_{abs} = \frac{D_{meas}^{ref}}{D_{sim}^{ref}} = (8.32 \pm 0.03) \times 10^{13} \tag{3}$$

per monitor unit. The validity of this method is based on the assumption, that the backscatter from the beam modifiers to the monitor unit ionization chambers is independent of the MLC and jaw settings. Therefore the energy deposit in the ionization chamber was scored for all simulated dose deliveries. The energy deposit in the ionization chambers per incident electron on the target was (260.6 ± 1.8) meV, averaged over all presented simulations ranging from equivalent square field sizes from 1 to 900 cm^2.

Standard deviations of the mean doses were scored using the history-by-history method [39,35,36]. History recycling was considered in the standard deviations with the latent variance approach, where a recycled history contributes to the deposited energy but is not counted as an individual history.

Material handling

In the Geant4 algorithm, the CT number information in Hounsfield units (HU) from the imported CT slices was converted into materials, following the approach of Schneider [40,26], by using 24 different elemental compositions for different CT number intervals in the range of human tissue HU ∈ [-1000,1600] and one material for metallic implants. To take the varying mass density with increasing HU values into account, a new G4material instance was created with a maximum density error of $\Delta\rho/\rho = \pm 0.5\%$, but at least every 10 HU, resulting in 114 G4material instances, which contained different material composition and mass density combinations. Voxels with Hounsfield unit values HU ≥ 1600 were assigned to contain pure titanium with a mass density of $\rho = 4.51$ g/cm^3. In MONACO the interaction properties within a voxel were calculated directly from the electron density without the need of an exact knowledge of the material composition [41,7]. The relative-to-water electron density values were obtained from the CT scanner Hounsfield values by a 15 point calibration curve [42]. The metallic implants were contoured explicitly and a structure was created. An electron density relative to water of 3.7 was assigned to the titanium structure. An artifact suppression algorithm was used to avoid a wrong Hounsfield unit assignment if reconstruction artifacts from metallic implants were present.

Measurements and simulations

Output factor measurements for fields larger than $(3 \times 3)\,cm^2$ as well as percentage depth dose curves were measured with an ionization chamber with 125 mm^3 detector volume (PTW 31010, Freiburg, Germany). The relative depth dose measurements were scaled with the output factors to obtain absolute doses. Lateral profile relative dose distributions and small field output factor measurements were performed with a diamond detector with 1-6 mm^3 detector volume (PTW 60003) and scaled with the central axis value of the corresponding depth dose curve in the respective depth. Seven different square fields with 1, 2, 3, 5, 10, 20 and 30 cm field length were measured and simulated at source surface distance SSD = 100 cm. In MONACO all fields on phantoms were simulated with a relative standard deviation of 0.5%. The Geant4 standard deviation for the square fields was 0.8% at 10 cm depth.

Film measurements and simulations were performed for an irregular MLC-shaped field with interdigitating MLC leaves in a solid water phantom at 5 cm water equivalent depth. Furthermore dose distributions of a $(5 \times 5)\,cm^2$ square field on a thorax phantom (CIRS model 002LFC), and a $(10 \times 10)\,cm^2$ square field on a pelvis phantom (CIRS model 002PRA) were evaluated. The Geant4 simulations of the pahntom cases had a standard deviation of 1.3% at 5 cm water equivalent depth. Film measurements were performed with Gafchromic EBT2 films (ISP, Wayne, USA). Films were digitized with an Epson (Tokyo, Japan) Expression 10000XL scanner. A Gafchromic EBT-easel was used for exact repositioning of the films on the scanner. In order to correct for the inhomogeneity of the light field [19,43], a scan of a non-irradiated film was made prior to film irradiation and was subtracted pixel-by-pixel from all irradiated films, including the calibration film. The obtained red channel intensity value I_{red} was fitted with equation (2) with three free parameters a, b and c, resulting in a coefficient of determination of $R^2 = 0.994$.

$$D(I_{red}) = \exp\left(\frac{I_{red} - a}{b}\right) - c \tag{2}$$

In order to compare dose distributions from both Monte Carlo simulations with film measurements in inhomogeneous

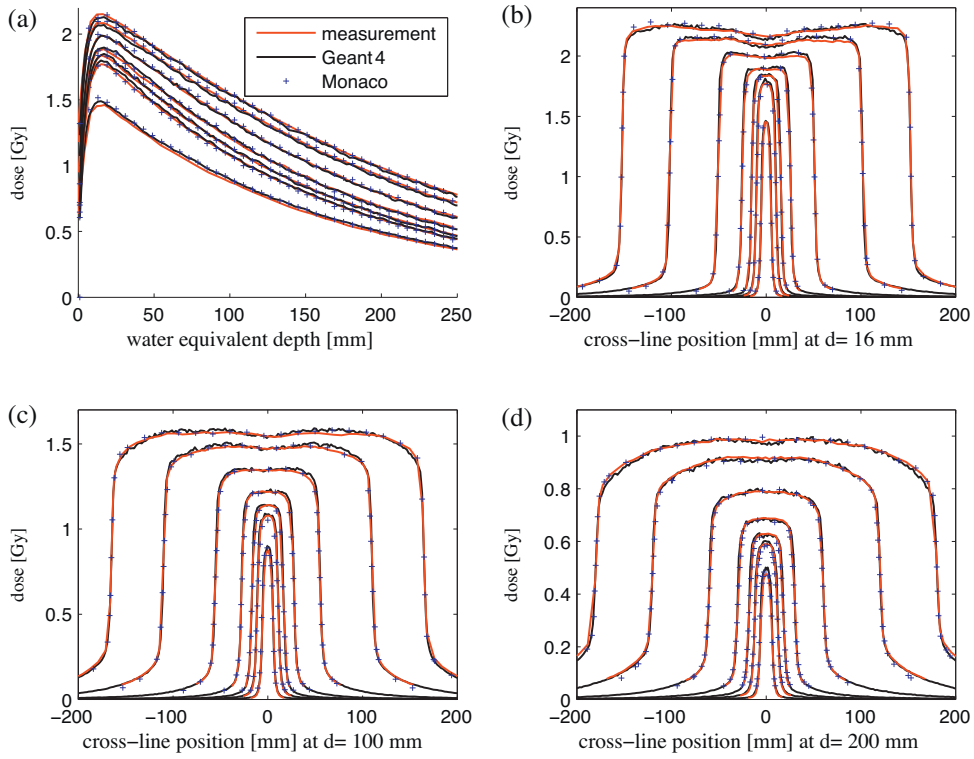

Figure 1. Geant4 (black lines), MONACO (blue crosses) and measured (red lines) depth dose curves are displayed in Figure 1a, while cross-line profiles for different square field sizes (1, 2, 3, 5, 10, 20, 30) cm at three different depths in water are displayed in Figures 1b-1d.

phantoms, the simulated dose distributions from MONACO and Geant4 were corrected by a dose-to-medium into dose-to-water correction factor $s_{w/m} = D_w/D_m$ [21,44], since the absolute dosimetric calibration of the films was performed in water equivalent material. A correction factor, was applied to every voxel in the dose cubes after the simulation (post processing) [45]. The material compositions and densities used to determine the correction factor were taken from Schneider et al. [40] and the unrestricted mass collision stopping power values were obtained at an electron energy of 0.9 MeV [21] using the ESTAR [46] database.

Data evaluation was performed with CERR[b], a Matlab (Mathworks, Natick, USA) based graphical user interface for radiotherapy applications and Omnipro I'mRT (IBA Dosimetry, Schwarzenbruck, Germany) for film evaluation and gamma analysis. The presented gamma pass rates [47] of the phantom and patient cases were calculated with 3% maximum dose deviation and 3 mm distance to agreement γ(3%, 3 mm) as a global index for all voxels above 25% of the maximum dose, with the reference dose being the maximum dose in the region of interest (ROI). The gamma pass rates of the beam commissioning were calculated with a local linear gamma with (2%, 2 mm) tolerance criteria.

[b] http://www.cerr.info.

VMAT treatment plans for comparisons on patient CT data

Two clinical VMAT treatment plans were analyzed in order to compare the Geant4 and MONACO dose calculation algorithms. The first case was a patient with stage IIIb lung cancer, where two primary tumors (lung segments 1 and 6) and one affected hilar lymph node in the right lung were present. The individual CTVs were combined into one non-convex PTV. The treatment was performed in 25 fractions with 2 Gy fraction dose, one 360° VMAT arc, 234 control points,651.1 MU, a total treatment time of 214 s and an equivalent square field size of $(4.67 \pm 2.39)^2$ cm^2. The patient received further treatment up to 66 Gy with a smaller PTV. The PTV covered 18% (355 cm^3) of the right lung volume. Hounsfield values within the PTV ranged from HU $\in$ [-800, 100].

The second patient received radiotherapy to the sixth thoracic vertebra T6, after spondylodesis. Since a previously irradiated volume (C6–T5) was present, sparing of the spinal cord was mandatory. A VMAT treatment with one 360° arc with 630.8 MU, 240 segments, an equivalent square field size of $(4.27 \pm 1.33)^2$ cm^2, a treatment time of 199 s and a prescription dose of 15 × 2 Gy was delivered. The PTV contained bone with up to 800 HU and titanium implants (>3000 HU). In MONACO, the metallic implant was contoured and a relative-to-water electron density of 3.73 was assigned to all voxels

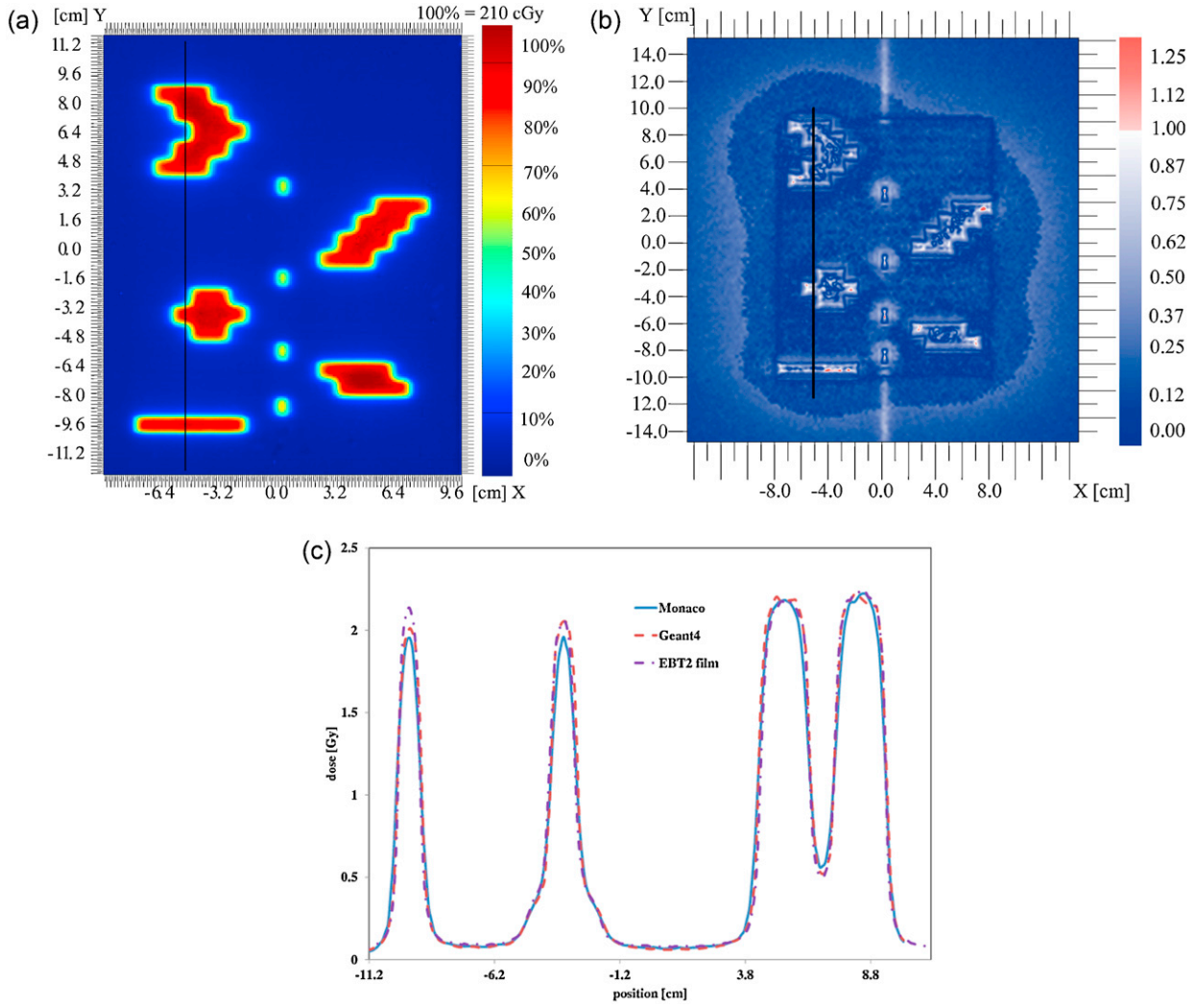

Figure 2. Irregular MLC-shaped field: dose distribution of the film measurement (2a), Geant4 versus MONACO gamma map (3%, 3 mm) (2b) and a profile in in-line direction at x = -5.3 cm (2c).

that belonged to this structure. In Geant4 all voxels with HU $\geq$ 1600 were assigned to be titanium with a mass density of $\rho_{Ti} = 4.51$ g/cm^3.

The relative standard deviation in the PTV of the MONACO simulations was $\sigma_{MONACO} = 0.4\%$, while the Geant4 simulations had a standard deviation of $\sigma_{Geant4} = 1.2\%$.

Results

A comparison between depth dose curves and lateral profiles at different depths is presented for measurements (red lines), Geant4 simulations (black lines) and MONACO simulations (blue crosses) in Figure 1. The gamma (2%, 2 mm) criterion had a mean pass rate of $(97.8 \pm 0.5)\%$ for the depth dose distributions of Geant4 versus measurements and $(96.8 \pm 1.5)\%$ for Monaco versus measurements in Figure 1a. Figures 1b-d show the respective profiles, in cross-line direction (parallel to the leaf motion) of the seven square fields at three different depths 16, 100 and 200 mm in water. The mean gamma (2%, 2 mm) pass rate for the lateral profiles was 95.8% for Geant4 versus measurement and 97.5% for Monaco versus measurements.

Figure 2a shows a dose distribution from a film measurement of the irregular MLC shaped segment. For γ(3%, 3 mm) a pass rate of 99.4% was found between the two dose calculation algorithms, 99.0% for film measurement against Geant4 and 97.3% for film measurement against MONACO. A Geant4 versus MONACO gamma agreement map (Figure 2b) and a profile in in-line-direction in Figure 2c demonstrate the agreement of the field penumbra in both directions, as well as the doses in the separate fields, within the simulation standard deviations and film measurement errors. Different regions of gamma agreement in the low dose region $D < 0.1\, D_{max}$ were identified in Figure 2b. The low dose region in the

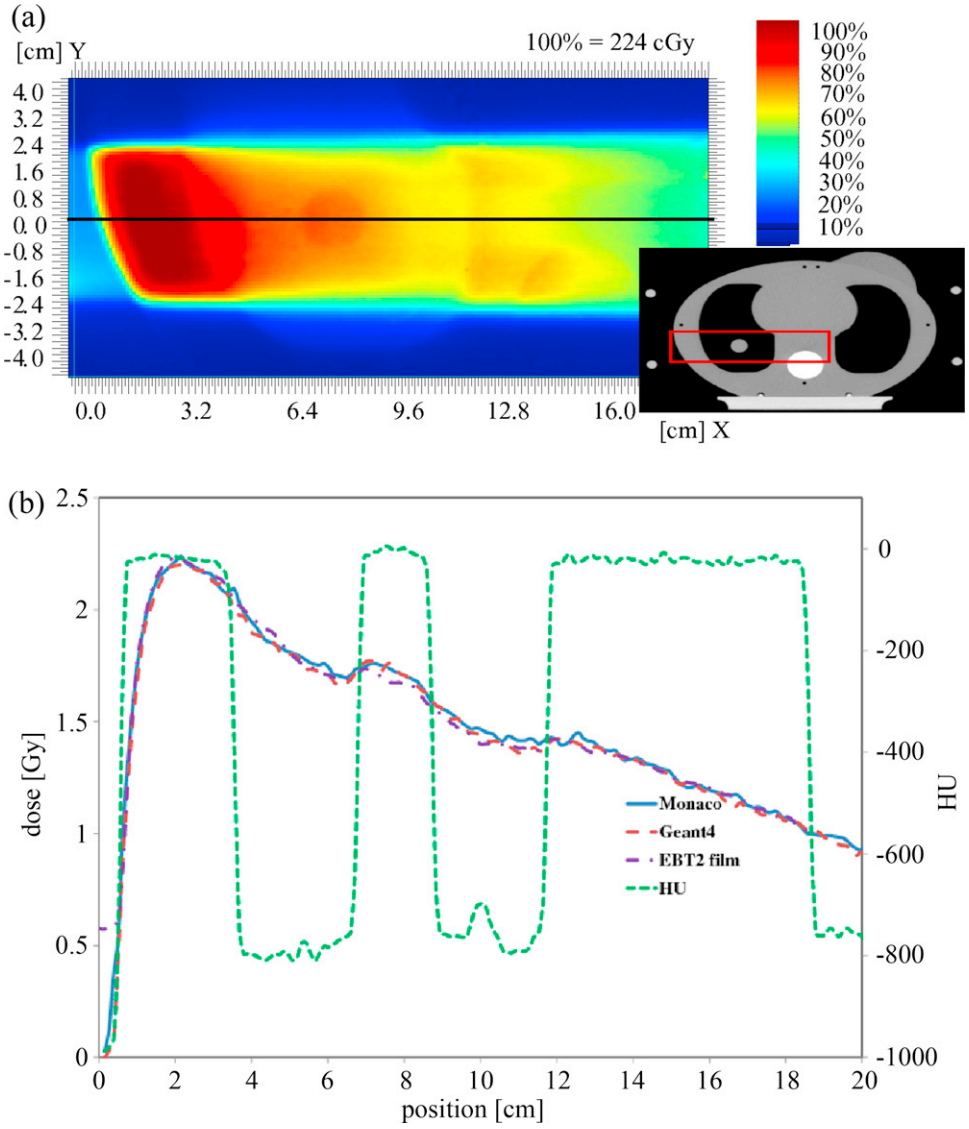

Figure 3. $(5 \times 5)\,cm^2$ square field delivered on a thorax phantom: transversal dose slice of a film measurement (3a) and dose profiles at $y = 0.3$ cm (3b).

central $(19 \times 16)\,cm^2$, where the deposited dose originated from photons transmitted solely through the MLC without backup jaws and scattered radiation, showed a gamma value of $\gamma = 0.13 \pm 0.04$. In this area the mean dose from Geant4 and MONACO was $(0.9 \pm 0.1)\%$ compared to the dose of an equivalent open field. This is in agreement with the measured transmission of the MLCi2 collimator, which was determined to be $(0.7 \pm 0.2)\%$ for an equivalent closed field, taken the additional scattered dose into account. Outside this area, the primary radiation was blocked by the MLC and jaws. The mean gamma value in this region was $\gamma = 0.33 \pm 0.06$, with Geant4 doses being higher than MONACO doses.

Figure 3a shows the dose distribution of a film measurement of a $(5 \times 5)\,cm^2$ square field, delivered on an inhomogeneous thorax phantom. A dose-to-water dose profile along the central axis of MONACO, Geant4 and film measurement is presented in Figure 3b. The Geant4 dose distributions had a gamma $\gamma(3\%, 3\,mm)$ pass rate of 99.2%, when compared to the film measurement and 98.4% when compared to MONACO. In regions with lung equivalent tissue, the mean gamma value was $\gamma = 0.45 \pm 0.27$, whereas in regions with soft tissue equivalence the mean gamma value was $\gamma = 0.26 \pm 0.17$. In analogy in Figure 4 the dose distribution of a $(10 \times 10)\,cm^2$ square field, delivered on an inhomogeneous pelvis phantom with a bone inlay and a dose profile are presented. The gamma pass rate of Geant4 versus film measurement was 97.0% and Geant4 versus MONACO 98.9%.

A transversal dose slice of the thoracic cancer VMAT treatment is shown in Figure 5a. The resulting DVHs for one

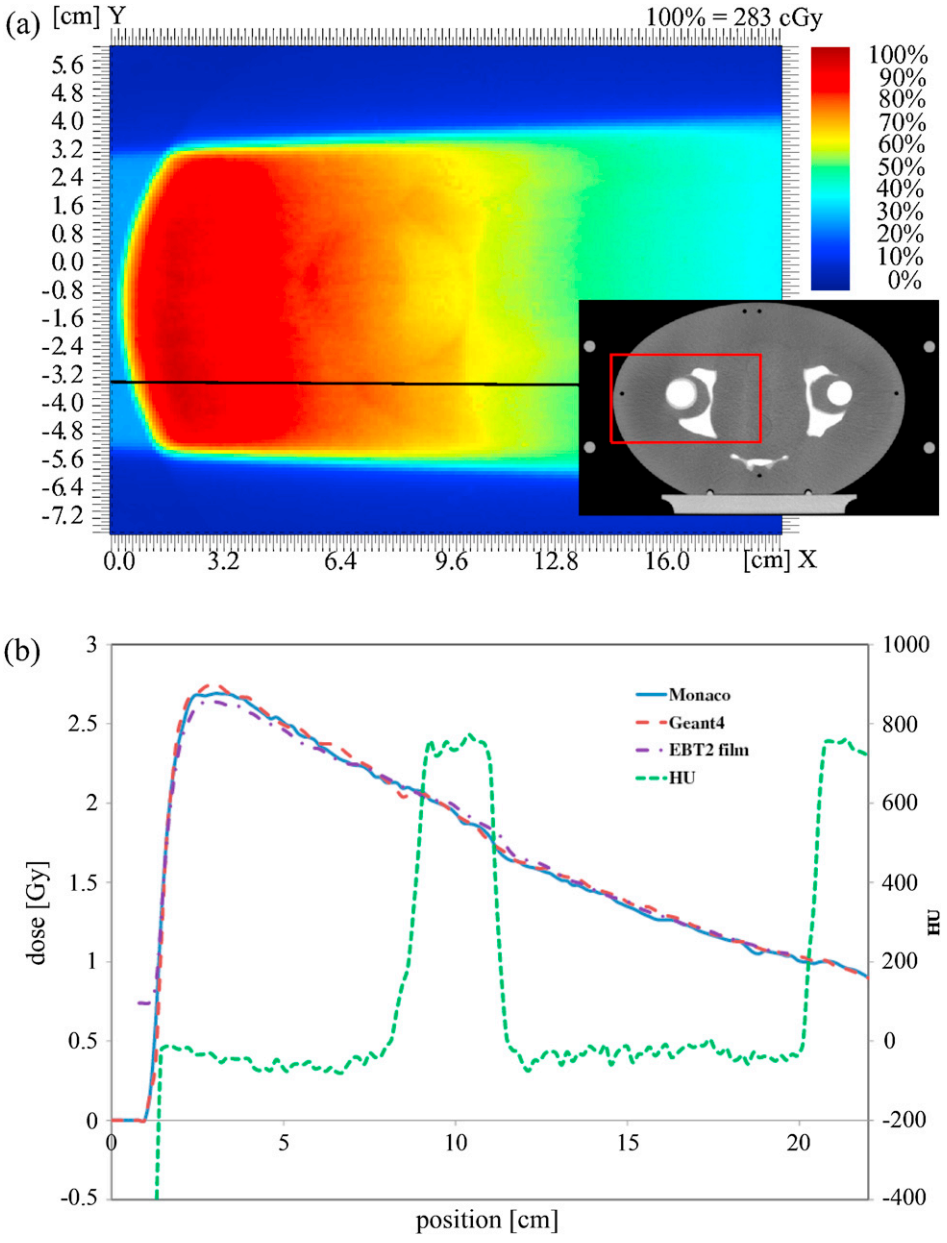

Figure 4. $(10 \times 10)\,cm^2$ square field delivered on a pelvis phantom: film measurement (4a) and dose profiles at y = -3.4 cm (4b).

treatment fraction for both dose calculation algorithms are presented in Figure 5b. The solid lines represent the MONACO dose distribution; the dash-dotted lines originate from the Geant4 dose distribution with the DICOM-RT plan file as input and the dashed lines originate from Geant4 with the linac logfile as input. The Geant4 performance was 83 hps for the dose calculation on DICOM data and 2.7×10^3 hps for the patient specific PHSP. This resulted in 1.2×10^2 h and 2.3×10^3 h runtime, divided by the number of computation cores, compared to 1.1 h for the Monaco dose calculation time on one node for the same standard deviation and grid size. The mean dose in the PTV in the Geant4 calculated dose distribution was -0.2% of the single fraction prescription dose if DICOM data was used as input and -0.3% if logfiles were used. The mean dose differences to the organs at risk (OAR) between Geant4 and MONACO were (0.6 ± 1.0)% and (0.4 ± 1.0)% of the single fraction prescription dose, with the trachea being the only OAR to receive less dose (-1.4% and -1.7%) in the Geant4 simulations. Line profiles through the PTV of the Geant4 DICOM (red dashed line), Geant4 logfile (purple dash-dotted line) and the MONACO (blue solid line) dose distributions are shown in Figure 5c. In addition the Hounsfield values are displayed (green dotted line). Figure 6a shows a transversal dose slice of the treatment in the thoracic

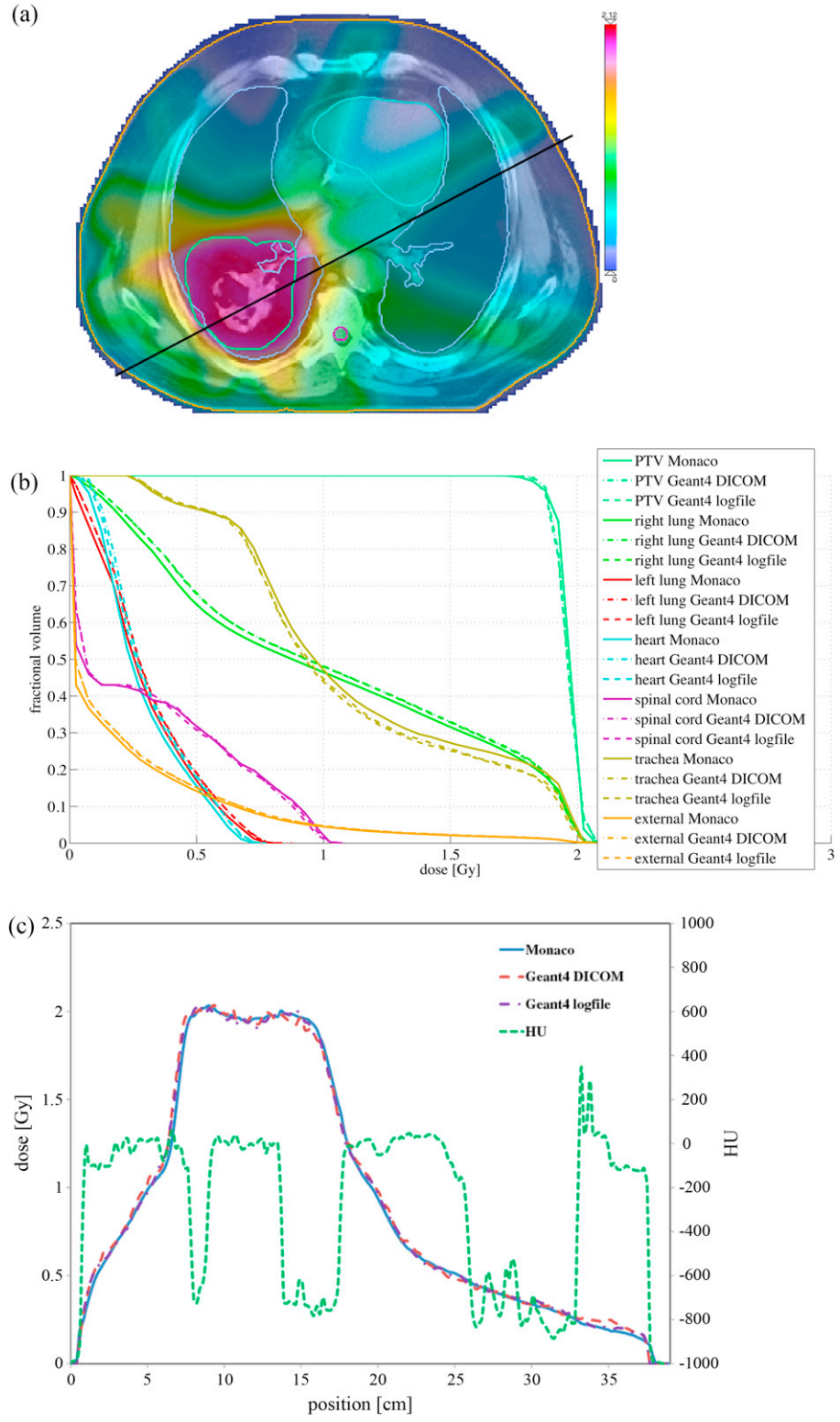

Figure 5. Thoracic tumor treatment: transversal slice of the dose distribution (5a), the resulting DVHs with MONACO, Geant4 DICOM and Geant4 logfile structure information (5b) as well as a profile through the PTV (5c).

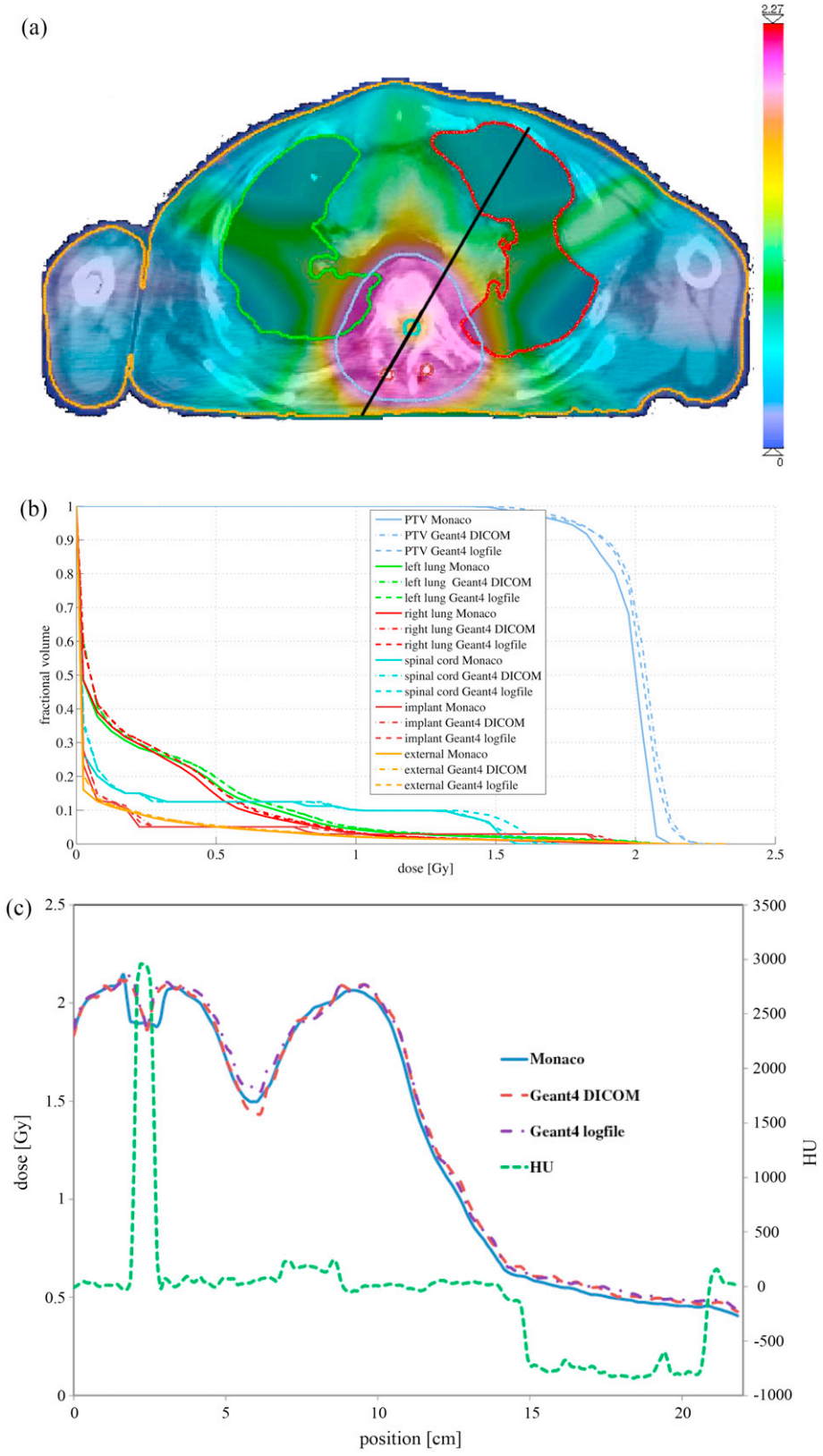

Figure 6. Spine region treatment: transversal slice of the delivered dose distribution (6a), DVHs with MONACO, Geant4 DICOM and Geant4 logfile structure information (6b) and a profile through the implants and the spinal cord (6c).

spine region. The DVH of the resulting dose distributions is presented in Figure 6b. The mean dose to the PTV was 2.0% and 1.7% higher in Geant4, while the mean deviations of the OAR-doses were $(1.9 \pm 1.2)\%$ and $(0.9 \pm 0.1)\%$. Figure 6c shows a profile of the resulting dose distributions through a metallic implant and the spinal cord.

Discussion

In order to evaluate the dosimetric accuracy of a treatment planning system used in clinical routine, an independent system of higher or at least comparable accuracy should be used. The presented Geant4 dose calculation algorithm neither makes use of information from MONACO nor does it rely on the variance reduction techniques used in XVMC code or a VEF model and can therefore be considered independent. With the presented evaluation an extension to the Grofsmid et al. [8] validation of MONACO was made, by including leaf interdigitation, a verification of a VMAT treatment delivery and dose deposits in arbitrary tissue with the option to convert into dose-to-water, as well as in realistic patient CT datasets.

For the depth dose curves deviations exceeding the tolerances were found in the buildup region, where no charged particle equilibrium was established [48] as well as for the $(1 \times 1)\,cm^2$ fields. Sauer et al. [18] and Sikora et al. [49] measured an output factor of 0.62 ± 0.10 for a $(0.8 \times 0.8)\,cm^2$ square field on an Elekta Synergy linear accelerator with beam modulator and a diamond detector. The output factor used in Figure 1 for the $(1 \times 1)\,cm^2$ field was 0.65, which is in agreement with the previous findings. Sikora et al. [49] pointed out the importance of an accurate modeling of the size of the primary photon source in the VEF model for the small field dose output. Therefore this parameter has to be determined as accurate as possible to be able to predict an accurate treatment outcome. Haryanto et al. [11] evaluated the dependency of the voxel size on the resulting output factor from Monte Carlo simulations for small fields. For both presented Monte Carlo simulations we had to integrate over the central 3 mm in each direction to achieve a good agreement with the measured profile. The manufacturer's tolerance for the diamond detector however was a radius less than 2 mm. For fields of and larger than $(10 \times 10)\,cm^2$ the Geant4 head model showed an under-dosage in the center of the radiation field and an over-dosage in the outer regions of the field which indicates a minor deviation in the mean beam energy or a different electron momentum distribution. In addition to that some voxels for the larger fields failed because of an asymmetry in the measured profiles, since Geant4 and Monaco created a symmetric dose output and the agreement was better on the left than on the right side.

The irregular MLC shaped field was used to demonstrate the penumbra of off-axis dose distributions shaped by the Elekta MLCi2 collimator in the case of overtraveling MLC-leaves. No deviations exceeding the tolerance criteria were found in the penumbra region for overtravelling leaves and standard leaf openings. The deviations in Figure 2c in the maximum dose values of the small fields originate from the different voxel positions in Geant4 and Monaco in combination with the high dose gradients in the presented region, since a good gamma agreement was found at these points in Figure 2b.Furthermore the agreement of the MLC transmission with and without jaws was demonstrated. If the radiation was blocked solely by the MLC an excellent agreement was found. A worse agreement was found in regions where the MLC and jaws blocked the radiation. In MONACO energy deposits were scored until the deposited dose in a voxel was below 0.5% of the maximum segment dose to save memory. The transmission through the jaws in in-line direction and the transmission through MLC plus backup-jaws were set to zero. In Geant4 particles were simulated as long as the energy and therefore the range in a certain material was above the range cut of 1 mm for electrons. All particles were tracked, independent of their position upstream of the MLC.

The square fields on inhomogeneous phantoms were used to compare the dose deposit in different density areas. Within the standard deviations a good agreement was found, however in agreement with Grofsmid et al. [8] the measurement and the Geant4 simulations yielded lower doses than the Monaco simulations in the lung equivalent tissue parts.

In the presented lung VMAT case deviations in the doses to the OARs originated from the summation of the MLC transmitted radiation. The OARs received higher doses due to the additional transmission contribution, whereas the PTV was treated predominantly with the primary beam. The trachea was the only OAR which received higher doses in Geant4 than in Monaco. This OAR contained voxels with Hounsfield units as low as -980 and deviations were therefore due to the different conversion methods of Hounsfield units into material properties.

For the presented Spine case deviations in the dose distribution at the implant outline originated from the different methods of assigning the material in Geant4 and MONACO. In MONACO every voxel that contained any fraction of the implant structure was assigned to the implant material. In Geant4 only voxels with Hounsfield units above 1600 were treated as titanium. Since the DVHs were created in CERR which assigns voxels according to their dominant structure, the Monaco PTV had voxel contributions from dose deposits in titanium.

Conclusion

In the presented VMAT cases, the resulting dose distributions from MONACO and Geant4 showed mean deviations of less than 2.0%. Therefore we conclude that the XVMC Monte Carlo algorithm in combination with the virtual energy fluence model, as implemented in MONACO is capable of predicting the dose distribution accurately over the whole range of human tissue densities even for highly modulated VMAT treatment arcs. Due to its short calculation time it can be fully applied for

clinical routine tasks. The presented Geant4 algorithm allows for detailed analysis of complex field geometries and electron density distributions during the commissioning process of a Monte Carlo treatment planning system and therefore enhances the possibilities to generate the optimal VEF model.

Acknowledgements

We would like to thank Kevin Brown (Elekta) for providing the construction data of the Elekta Synergy linear accelerator treatment head. This work was in part funded by a research grant from Elekta and by the bwGRiD portal project of Baden-Württemberg.

References

[1] Jahnke L, Fleckenstein J, Wenz F, Hesser J. GMC: a GPU implementation of a Monte Carlo dose calculation based on Geant4. Phys Med Biol 2012;27:1217–29.
[2] Jia XGX, Graves YJ, Folkerts M, Jiang SB. GPU-based fast Monte Carlo simulation for radiotherapy dose calculation. Phys Med Biol 2011;56:7017–31.
[3] Vynckier S, Heijman BJM, van Dijk E, Zoetelief J, Bos A JJ, Lammertsma AA, et al. Netherlands Commission on Radiation Dosimetry. Monte Carlo treatment planning: An introduction 2006.
[4] Fippel M, Haryanto F, Dohm O, Nüsslin F, Kriessen S. A virtual energy fluence model for Monte Carlo dose calculation. Med Phys 2003;30:301–11.
[5] Sikora M, Alber M. A virtual source model of electron contamination of a therapeutic photon beam. Phys Med Biol 2009;54:7329–44.
[6] Fippel M. Fast Monte Carlo dose calculation for photon beams based on the VMC electron algorithm. Med Phys 1999;26:1466–75.
[7] Kawrakow I, Fippel M, Friedrich K. 3D electron dose calculation using a Voxel based Monte Carlo algorithm (VMC). Med Phys 1995;23:445–57.
[8] Grofsmid D, Dirkx M, Marijnissen H, Woudstra E, Heijmen B. Dosimetric validation of a commercial Monte Carlo based IMRT planning system. Med Phys 2010;37:540–9.
[9] Stieler F, Wolff D, Schmid H, Welzel G, Wenz F, Lohr F. A comparison of several modulated radiotherapy techniques for head and neck cancer and dosimetric validation of VMAT. Radiother Oncol 2011;101:388–93.
[10] LoSasso T, Chui C, Ling C. Physical and dosimetric aspects of a multileaf collimation system used in the dynamic mode for implementing intensity modulated radiotherapy. Med Phys 1998;25:1919–27.
[11] Haryanto F, Fippel M, Laub W, Dohm O, Nüsslin F. Investigation of photon beam output factors for conformal radiation therapy- Monte Carlo simulations and measurements. Phys Med Biol 2002;47:N133–43.
[12] Teke T, Bergman AM, Kwa W, Gill B, Duzenli C, Popescu A. Monte Carlo based, patient specific RapidArc QA using linac log files. Med Phys 2010;37:116–23.
[13] Pisaturo OMR, Mirimanoff R-O, Bochud FO. A Monte Carlo based procedure for independent monitor unit calculation in IMRT treatment plans. Phys Med Biol 2009;56:7017–31.
[14] Boggula R, Birkner M, Lohr F, Steil V, Wenz F, Wertz H. Evaluation of a 2D detector array for patient-specific VMAT QA with different setups. Phys Med Biol 2011;56:7163–77.
[15] Nelms BE, Zhen H, Tome WA. Per-beam, planar IMRT QA passing rates do not predict clinically relevant patient dose errors. Med Phys 2011;38:1037–44.
[16] Kruse JJ. On the insensitivity of single field planar dosimetry to IMRT inaccuracies. Med Phys 2010;37:2516–24.
[17] Schwedas MSM, Wiezorek T, Wendt TG. Strahlenphysikalische Einflussgroeßen bei der Dosimetrie mit verschiedenen Detektortypen. Z Med Phys 2007;17:172–9.
[18] Sauer OA, Wilbert J. Measurement of output factors for small photon beams. Med Phys 2007;34:1983–8.
[19] Menegotti L, Delana A, Martignano A. Radiochromic film dosimetry with flatbed scanners: A fast and accurate method for dose calibration and uniformity correction with single film exposure. Med Phys 2008;35:3078–85.
[20] Schneider F, Polednik M, Wolff D, Steil V, Delana A, Wenz F, et al. Optimization of the gafchromic EBT protocol for IMRT QA. Z Med Phys 2009;19:29–37.
[21] Siebers JV, Keall PJ, Nahum AE, Mohan R. Converting absorbed dose to medium to absorbed dose to water for Monte Carlo based photon beam dose calculations. Phys Med Biol 2000;45:983–95.
[22] Agostinelli S, Allison J, Amako K, Apostolakis H, Araujo H, Arce Dupois P, et al. Geant4 - A Simulation Toolkit. Nucl Instr and Meth A 2003;506:250–303.
[23] Allison J, Amako K, Apostolakis H, Araujo H, Arce Dubois P, Asai M, et al. Geant4 Developments and Applications. IEEE Transactions on Nuclear Science 2006;53:270–8.
[24] Jan S, Benoit D, Becheva E, Carlier T, Cassol F, Descourt D, et al. GATE V6: a major enhancement of the GATE simulation platform enabling modelling of CT and radiotherapy. Phys Med Biol 2010;56:881–901.
[25] Grevillot L, Frisson T, Maneval D, Zahra N, Badel JN, Sarrut D. Simulation of a 6 MV Elekta Precise Linac photon beam using GATE/GEANT4. Phys Med Biol 2011;56:903–18.
[26] Paganetti H, Jiang H, Parodi K, Slopsema R, Engelsman M. Clinical implementation of full Monte Carlo dose calculation in proton beam therapy. Phys Med Biol 2008;53:4824–53.
[27] Fleckenstein J, Jahnke L, Petersheim M, Hesser J, Wenz F. Klinische Implementation von Geant4 zur Verifikation komplexer IMRT-Dosisverteilungen eines Elekta Synergy Linearbeschleunigers. Int J Radiat Oncol Biol Phys 2009;185:128–9.
[28] Wertz H, Jahnke L, Schneider F, Polednik M, Fleckenstein J, Lohr F, et al. A novel lateral disequilibrium (LDI) pencil-beam based dose calculation algorithm: Evaluation in inhomogeneous phantoms and comparison with Monte Carlo simulations. Med Phys 2011;38:1627–34.
[29] Baro J, Sempau J, Fernandez-Varea JM, Salvat F. PENELOPE: An algorithm for Monte Carlo simulation of the penetration and energy loss of electrons and positrons in matter. Nucl Instr and Meth B 1995;100:31–46.
[30] Wright DH. Physics Reference Manual Version: geant4 9.4. Geant4 Collaboration 2010.
[31] Urban L. A multiple scattering model *CERN OPEN 2006-077*, 2006.
[32] Paganetti H. Four-dimensional Monte Carlo simulation of time-dependent geometries. Phys Med Biol 2004;49:N75–81.
[33] Gabriel E, Fagg G, Bosilca G, Angskun T, Diongarraa JJ, Squyres M, et al. OpenMPI: Goals, Concept, and Design of a next generation MPI Implementation. In: Proceedings, 11th European PVM,MPI Users' Group Meeting. 2004.
[34] Tzedakis A, Damilakis JE, Mazonakis M, Stratakis J, Varveris H, Gourtsoyiannis N. Influence of initial electron beam parameters on Monte Carlo calculated absorbed dose distributions for radiotherapy photon beams. Med Phys 2004;31:907–13.
[35] Chetty IJ, Curran B, Cygler JE, DeMarco JJ, Ezzell G, Faddegon BA, et al. Report of the AAPM Task Group No. 105: Issues associated with clinical implementation of Monte Carlo-based photon and electron external beam treatment planning. Med Phys 2007;34:4818–53.
[36] Walters BRB, Kawrakow I, Rogers DW. History by history statistical estimators in the BEAM code system. Med Phys 2002;29:2745–52.
[37] Popescu IA, Shaw CP, Zavgorodni SF, Beckham WA. Absolute dose calculations for Monte Carlo simulations of radiotherapy beams. Phys Med Biol 2005;50:3375–92.
[38] Ma CM, Price Jr RA, Li JS, Chen L, Wang L, Fourkal E, et al. Monitor unit calculation for Monte Carlo treatment planning. Phys Med Biol 2004;49:1671–87.
[39] Sempau J, Sanchez-Reyes A, Salvat F, Ben Tahar HO, Jiang SB, Fernández-Varea JM. Monte Carlo simulation of electron beams from an accelerator head using PENELOPE. Phys Med Biol 2001;46:1163–86.

[40] Schneider W, Bortfeld T, Schlegel W. Correlation between CT numbers and tissue parameters needed for Monte Carlo simulations of clinical dose distributions. Phys Med Biol 1999;45:459–78.
[41] Fippel M, Nüsslin F. Bestimmung der Wechselwirkungsparameter des menschlischen Gewebes für Monte-Carlo-Dosisberechnungen in der Strahlentherapie. Strahlenther Onkol 2001;177:206–11.
[42] Vanderstraeten B, Chin P, Fix M, Leal A, Mora G, Reynaert N, et al. Conversion of CT numbers into tissue parameters for Monte Carlo dose calculations: a multi-centre study. Phys Med Biol 2007;52:539–62.
[43] Saur S, Frengen J. Gafchromic EBT film dosimetry with flatbed CCD scanner: A novel background correction method and full dose uncertainty analysis. Med Phys 2008;35:3094–101.
[44] Fernández-Varea J, Carrasco P, Panettieri V, Brualla L. Monte Carlo based water/medium stopping-power ratios for various ICRP and ICRU tissues. Phys Med Biol 2007;52:6475–83.
[45] Dogan N, Siebers JV, Keall PJ. Clinical comparison of head and neck and prostate IMRT plans using absorbed dose to medium and absorbed dose to water. Phys Med Biol 2006;51:4967–80.
[46] Berger MJ, Coursey JS, Zucker MA, Chang J. Stopping Power and range tables for electrons, protons and helium ions, 1998. http://physics.nist.gov.
[47] Low DA, Harms WB, Mutic S, Purdy JA. A technique for the quantitative evaluation of dose distributions. Med Phys 1998;25:656–61.
[48] Kawrakow I. On the effective point of measurement in megavoltage photon beams. Med Phys 2006;33:1829–39.
[49] Sikora M, Dohm O, Alber M. A virtual photon source model of an Elekta linear accelerator with integrated mini MLC for Monte Carlo based IMRT dose calculation. Phys Med Biol 2007;52:4449–63.